Energy for Sustainable Development 34 (2016) 100–110

Contents lists available at ScienceDirect

Energy for Sustainable Development

Study on energy conversion and storage system for a prototype buoys-array wave energy converter

Zhen Liu [a,b,*], Na Qu [c], Zhi Han [c], Jiaming Zhang [c], Shuai Zhang [c], Ming Li [a,b], Hongda Shi [a,b]

[a] Shandong Provincial Key Laboratory of Ocean Engineering, Ocean University of China, China
[b] Qingdao Municipal Key Laboratory of Ocean Renewable Energy, Ocean University of China, China
[c] College of Engineering, Ocean University of China, China

ARTICLE INFO

Article history:
Received 7 August 2015
Revised 24 April 2016
Accepted 27 July 2016
Available online xxxx

Keywords:
Wave energy
Buoys-array
Hydraulic accumulator system
Experimental validation
Numerical simulation
Wave-to-wire

ABSTRACT

Wave power in China has an energy density that is one-tenth of that of the wave power in Europe. Therefore, Chinese developers cannot simply replicate and transplant European devices and facilities to East Asia. Instead, to exploit the conditions in East Asia, a combined-oscillating-buoy-based wave energy convertor (WEC) is proposed as an array-type WEC. Sea trials of a 10 kW pilot device confirmed the feasibility of its buoy array and hydraulic pressure system (HPS) for wave-energy conversion. Field test data indicated that the energy-converting efficiency of the direct-drive design was relatively low, suggesting the urgency of developing energy storage systems to the increase of power take-off productivity. A hydraulic accumulator system (HAS) was designed to replace the original direct-drive operating mechanism for a 100 kW final-prototype device. It was expected that the system will exhibit an improved ability to collect and store energy from smaller waves to enhance the total converting efficiency. Experimental studies were performed to investigate the hydrodynamic characteristics of the heaving buoys under the damping effects, and the operating performance of the accumulator system. A numerical wave-to-wire model based on Simulink, Matlab was set-up to study the energy output of the HPS-HAS under the wave conditions of the test site. It was shown that four buoys could charge ten accumulators in half an hour under local actual sea conditions. Furthermore, in a same running time, the output energy of the HPS-HAS is over forty times larger than that of the HPS without any energy storage device. In addition, energy discharging from three accumulators only could reach about 20 kW output power. The numbers of buoys and accumulators should be optimized to improve wave-energy storage and power generation in the future.

Introduction

Wave energy is one of the most important offshore forms of renewable energy. The global wave energy potential is of the same order of magnitude as the world's consumption of electricity energy (Cruz, 2008). The exploitable limit of this resource is approximately 10–25% (Melo and Huckerby, 2011). Marine energy, including wave energy, is also believed to have the potential to play an important role in the future electricity mix in China. As a result, 200 million RMB per year have been allocated from the centre budget since 2010 to financially support the development of ocean renewable energy through State Ocean Administration (SOA) (NOTC, 2014).

Compared to traditional wave-energy-converting technologies such as the oscillating water column and overtopping devices, the oscillating-body type wave energy converter (WEC) is classified as a 3rd generation device (Falcão, 2010). Its advantage is the ability to work in the deep sea to capture more wave power. A heaving buoy was proposed as an oscillating-body wave energy device, which is also called a point absorber (Astariz and Iglesias, 2015). Furthermore, a two-body heaving buoy was suggested to operate against the tide oscillations (Titah-Benbouzid and Benbouzid, 2014). In addition, a many-body system with arrays of oscillating buoys was tested in a wave basin to study the feasibility study of a wave farm (Stratigaki et al., 2014). Through a grant from SOA, Ocean University of China (OUC) developed a 10 kW buoys-array pilot WEC as the phased achievement of the final aim, which is a 100 kW prototype device. It comprises four normal-sized buoys instead of one large floater, in order to capture more wave energy under low-density conditions (Shi et al., 2016).

In order to convert the energy captured by the heaving buoy, two direct-driving technologies, namely, a rack & pinion system and a linear generator have been proposed and used. In the rack & pinion system, the ratchet wheels are used to cause the unidirectional rotation of the generator (Zhang et al., 2012). Because of the unavoidable mechanical-fragility resulting from the expansion of the buoy size, the rack & pinion

* Corresponding author at: Qingdao Municipal Key Laboratory of Ocean Renewable Energy, Ocean University of China, China.
E-mail address: liuzhen@ouc.edu.cn (Z. Liu).

http://dx.doi.org/10.1016/j.esd.2016.07.004
0973-0826/

system was found to be employed only in small WECs with an installed capacity of 1 kW at most (Liu et al., 2015). The linear generator, which used a permanent magnet, was employed in a few heaving-buoy WEC prototypes (Leijon et al., 2005; Polinder et al., 2005; Elwood et al., 2010). Recently, a linear generator was designed and tested for an installed capacity as high as 50 kW (Hodgins et al., 2012). A control method to improve the performance of linear generators was proposed by Nie et al. (2013). The effects of electrical damping of the linear generator on the optimization of the power output were elucidated by Ekstrom et al. (2015).

Another method to convert the wave energy transmitted by the heaving buoy is to employ a hydraulic pressure system (HPS) (Hong et al., 2014). A HPS can adapt better to the slow motion of WECs (Pizer et al., 2005; Haun, 2015), and smoothen the irregular fluctuations in the random-wave energy using an oil/gas accumulator (Lopez et al., 2013). Therefore, the HPS were applied in different kinds of WECs, such as Pelamis (Henderson, 2006), Pendulum (Lin et al., 2013), Wavestar (Hansen et al., 2013), and Duck (Zhang et al., 2014). The feasibility and reliability of HPSs and accumulators have been proven through in-house experiments and actual sea trials.

The motions of the oscillating bodies of a WEC are strongly affected by the variation in the pressure of the HPS. The interactions between the wave-driven bodies and the power take-off (PTO) modules of the HPS have significant effects on the energy-conversion efficiency of the WEC. As the desktop tool, a mathematical model based on a simplified mass-spring-damper system was employed to simulate the interaction of the HPS and an oscillating buoy (Falcão, 2007). Based on this assumption, a few real-time control techniques and optimization strategies were proposed for improving the PTO efficiency (Li et al., 2012; Fusco and Ringwood, 2013; Abraham and Kerrigan, 2013; Cargo et al., 2014; Sheng et al., 2014; Clement and Babarit, 2012). In addition, the latching control method was found to be suitable for enhancing the wave-energy

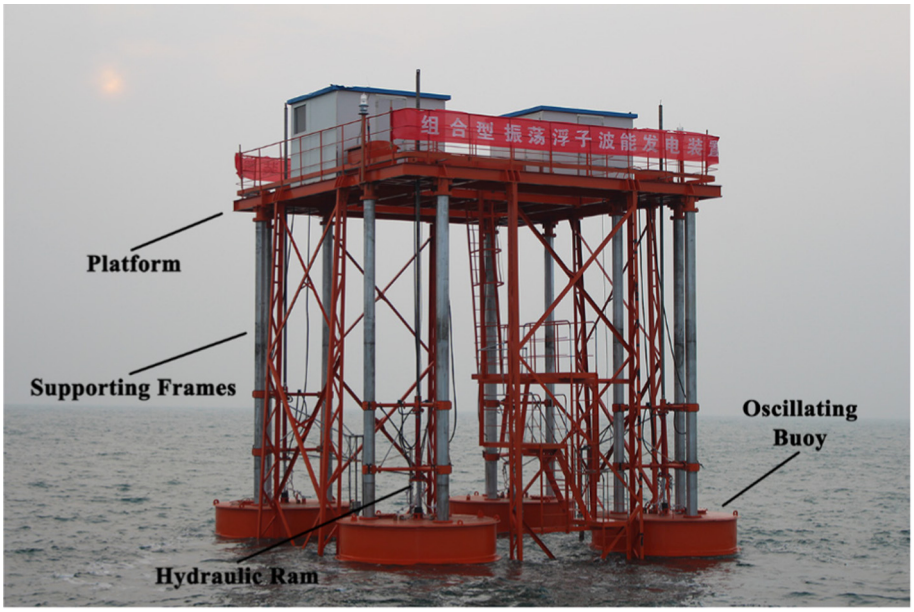

(a) WEC on-site

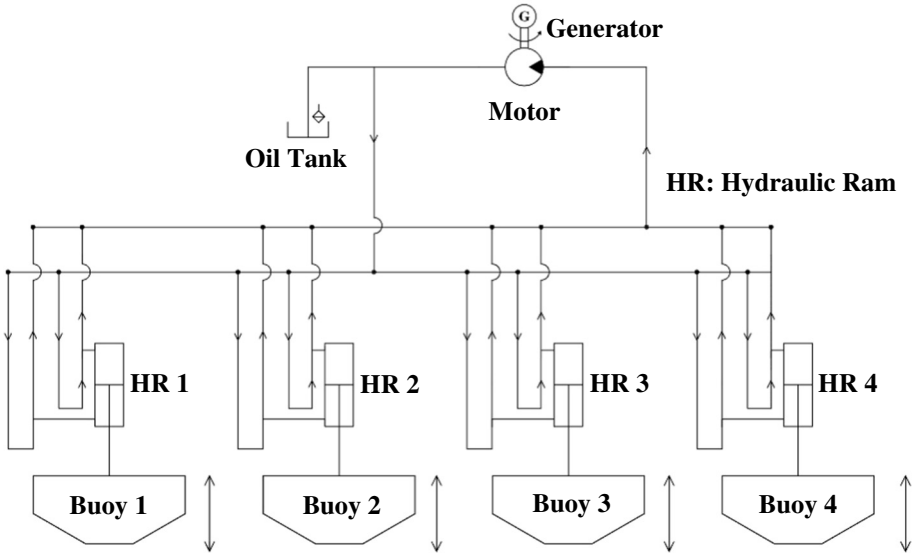

(b) Schematic of HPS

Fig. 1. 10 kW oscillating-buoys-array WEC in operation at test site.

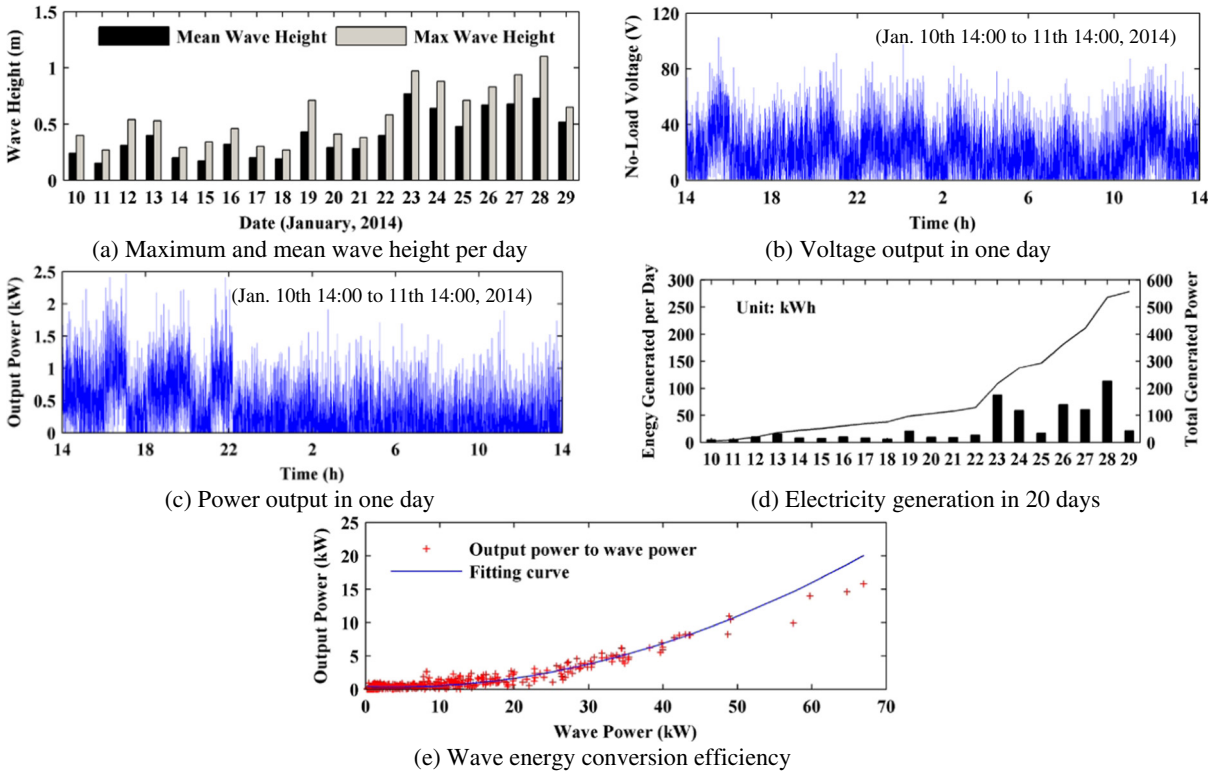

Fig. 2. Sea trial data for 10 kW prototype WEC.

conversion efficiency; however, it made the controlling system more complicated (Falcão, 2008; Sheng et al., 2015). It should be noted that most of these numerical models focused on the hydrodynamics of the heaving buoys under effects of the HPS. On the other hand, there have been few reports on the operating performance of the HPS and accumulators with respect to buoys.

In contrast to computer programs, laboratory experiments can provide more convincing and useful data for designers and engineers (Choi et al., 2012; Lasa et al., 2012). Based on the validation of experimental data, a numerical model called "wave-to-wire" can realize the prediction from the incident wave energy to the output electrical-power directly under specific devices, including SEAREV (Josset et al., 2007), the hyperbaric converter (Garcia-Rosa et al., 2014), the oscillating water column device (Kelly et al., 2015) and the array of WEC (Forehand et al., 2016). The energy transmission, loss, and related dynamic interactions between each two energy converting stages can be all considered during these calculations. Compared to the former numerical models which only can deal with an individual energy-converting stage, the wave-to-wire model is a promising desktop method for fully understanding of the performance of the wave energy converter.

From the presented literature review, it is clear that few studies have investigated the operating performance the hydraulic accumulator system (HAS) coupled with the HPS for wave energy conversion. Further, the related wave-to-wire model of the combined heaving-buoys WEC has not been studied extensively. In this study, the sea trial data of the 10 kW pilot WEC is analyzed to demonstrate the importance of HAS in the low-wave-energy density conditions. Further, a new hydraulic system for the 100 kW final-prototype WEC is designed and investigated. An accumulator system is coupled to the HPS to store and transmit the hydraulic power. Laboratory experiments for the heaving buoys and HAS are conducted for feasibility analysis. A wave-to-wire model based on Matlab Simulink is developed and validated using the experimental data. Numerical simulations of the energy-conversion and storage system are carried out. Finally, the performance of the HPS-HAS system with respect to the energy charging and discharging is analyzed for further optimization.

Sea trials of 10 kW pilot WEC

A pilot WEC rated to 10 kW and developed by OUC was deployed at the test site, which is located at the south of Zhaitang Island, on January 10, 2014. As shown in Fig. 1 (a), a cubic frame was employed to support the four oscillating buoys. A submerged floating body was fixed to the frame bottom to provide buoyancy and keep the frame motionless. The frame was also connected to a concrete ballast using steel wires and ultrahigh-molecular-weight polyethylene ropes. A 500-ton crane boat, used in conjunction with a semi-submerged barge, deployed the device and the ballast together. This technology is also available for future salvage operations.

As shown in Fig. 1 (b), a hydraulic ram was installed on the top of each buoy. During the oscillation of the buoys, the hydraulic rams could operate such that they exhibited both up and down motions. The high-pressure oil from four buoys was collected directly to drive the hydraulic motor on the platform without using any accumulator.

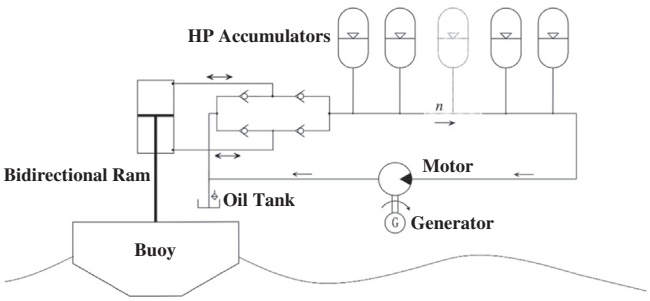

Fig. 3. Accumulators in the hydraulic power transmission system.

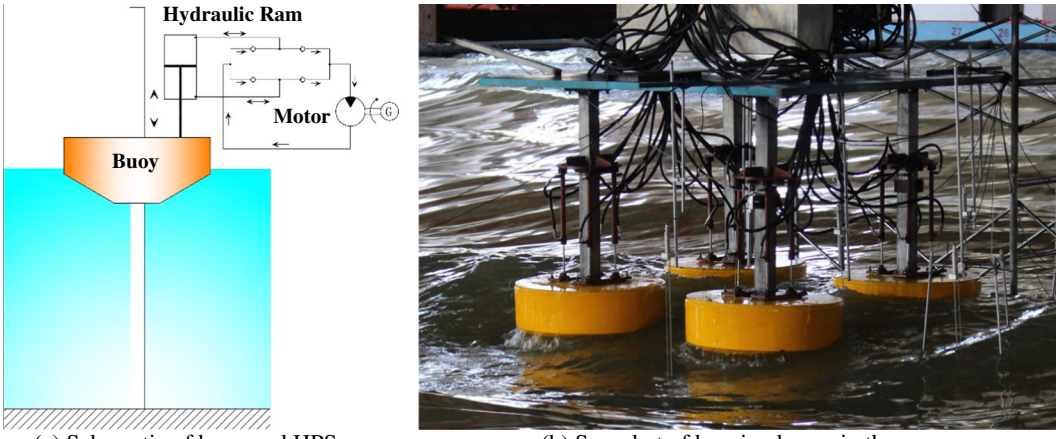

(a) Schematic of buoy and HPS (b) Snapshot of heaving buoys in the waves

Fig. 4. Hydrodynamic experiment for heaving buoys under damping effects of HPS.

An electricity control & management system presented on the platform was used to consume all the generated electricity on-site. Four heaving buoys were originally expected to oscillate in different phases under incident wave conditions to generate relatively constant oil flows to drive the generator.

The data from a series of sea trials are shown in Fig. 2. The recording period was 20 days, extending from January 10 to 29, 2014, immediately after the deployment of the device. As illustrated in Fig. 2 (a), the mean wave height, H_m, from 10th January to 22nd January was 0.38 m, which is typical for winter in this sea area. This value increased to 0.65 m during the next week because of two gales. The no-load voltage during a single day (14:00, January 10 to 14:00, January 11, 2014) is displayed in Fig. 2 (b). The maximum voltage did not exceed 110 V. Although the device could operate under the low-wave-energy-density conditions (H_m = 0.38 m, H_{max} = 0.64 m), the maximum and mean values of the output power were only 2.46 kW and 0.36 kW, respectively (see Fig. 2 (c)). As shown in Fig. 2 (d), the average power generated per day from 10th January to 22nd January was 0.43 kWh and 2.55 kWh in the next week. The accumulative electricity power in this period was 557 kWh. The relationship between the time-averaged (1 h) electric power and wave power is shown in Fig. 2 (e); the curve shows 480 points for 20 days. The mean energy-conversion efficiency was 18.2%, which is close to the efficiency in the initial design.

The mean wave height during this period was smaller than the annual-averaged value of 0.6 m. This indicates that the heights of dominant waves were quite small. On the other hand, the hydraulic system required a continuous flow of oil at a high-pressure to keep the hydraulic motor rotating at a constant speed, in order to ensure a better electricity output. Although some large waves could drive the WEC to generate a few high-pressure peaks, the wave train was unable to provide a constant flow of oil to keep the generator rotating. The generator was kept in the start/stop switching status, which resulted in a low operational-efficiency.

The direct output voltage could not meet the battery-charging or local grid-transformation demands. In order to fully utilize all the discrete high-pressure peaks, an energy storage system with an accumulator is required (Falcão, 2007; Shi et al., 2016). The bladder accumulator can collect all the small oil flows at high pressures and then release them continuously (Gaspar et al., 2015). Based on the data collected from the sea trials of the 10 kW pilot WEC and the results of previous studies, a new energy conversion and storage system was designed for the final-prototype WEC. The HPS was equipped with a HAS to satisfy the demands of high pressure oil flows to drive the 100 kW generator. The HAS was responsible for collecting all the discrete high-pressure flows from the hydraulic rams under the low-wave-energy-density conditions.

Energy conversion and storage system

System design

The accumulators were used as the key facilities to store the incident wave energy in the front end in the form of hydraulic power, as shown in Fig. 3. The accumulators were connected to the hydraulic motor instead of the hydraulic rams in order to reduce the fluctuations in the pressure and the flow rate and ensure a better electrical-power output. The number of accumulators was chosen so as to balance the conflict between the energy charging and discharging periods.

The HAS divides the hydraulic-power transmission process into two stages: energy charging and discharging. In the energy charging stage, it is important to set the upper/lower limits of accumulators based on the buoy-driven forces, which, in turn, are determined by the maximum energy of the incident waves. The requirements of the hydraulic motor

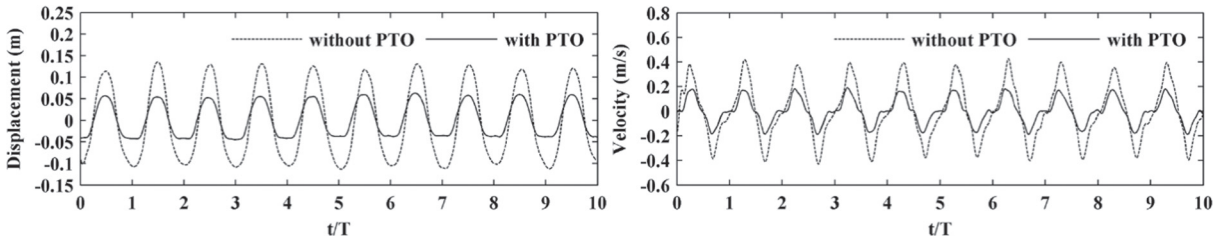

(a) Displacement (b) Velocity

Fig. 5. Time histories of displacements and velocities of heaving buoy (H = 0.20 m, T = 2.5 s).

with respect to the hydraulic pressure and oil flow rate also should be considered and be in keeping with the rated power of the electrical generator.

During the energy-discharging stage, the output electric-quantity can be considered as an estimating standard. In addition, the voltage of the generator should stay above the threshold for battery charging. Frequent start/stop switching of the hydraulic motor should be avoided. A continuous flow of oil at high pressures depends on the oil-release controlling strategy of the various accumulators.

Experimental tests of heaving buoys

In order to investigate the dynamic characteristics of heaving buoys under the damping effects of the HPS, a hydrodynamic experiment for a four-buoy array was performed in a wave basin, located in the Ocean University of China. Each buoy was connected to the HPS through four hydraulic rams, as shown in Fig. 4 (a). The shape parameters of the gyro-like buoys included the upper cylinder diameter of 0.9 m and height of 0.375 m and the bottom inverted-cone height of 0.25 m. Regular waves were employed as incident waves. The wave height H varied from 0.15 m to 0.25 m, and the period T varied from 1.5 s to 2.5 s. The displacement of the hydraulic motor was 8.2 cm^3 per revolution. The installed capacity of the generator was 50 W. A snapshot of the heaving buoys in the waves is shown in Fig. 4 (b).

As shown in Fig. 5 (a), the typical time history of the displacement of the left-hand front-row buoy under the damping effects of the HPS (with PTO) is compared with that of a free-oscillating buoy (without PTO). The incident wave height was 0.20 m, and the period was 2.5 s. The position of the buoy was measured by a linear displacement sensor. The displacement curve of the free oscillation is very close to sinusoidal in shape. The peak height of the curve with PTO effects decreased to approximately half of the free oscillation. Moreover, the lag phenomena are observed when the buoy moves to the bottom. While the buoy at the top has the gravity as a recovery force, the buoy at the bottom requires a longer time for a larger wave force to restart and move up.

Accordingly, the linear velocity can be directly derived from the time derivative of the displacement. As shown in Fig. 5 (b), the curves both with and without PTO effects present pseudo-sinusoidal shapes. The positive and negative peaks in velocity with the PTO effects are also approximately half of those for the free- oscillation velocity. The steps at the zero points of the curve with the PTO effects are caused by the lag of the buoy at the bottom of the displacement cycle. The heaving buoys under other wave conditions also showed behaviours similar to those observed in Fig. 5.

A comparison of mean velocities between the buoys in the front and rear rows is shown in Fig. 6. The difference in mean velocity for the buoys in the front and rear rows is small. Most differences under various

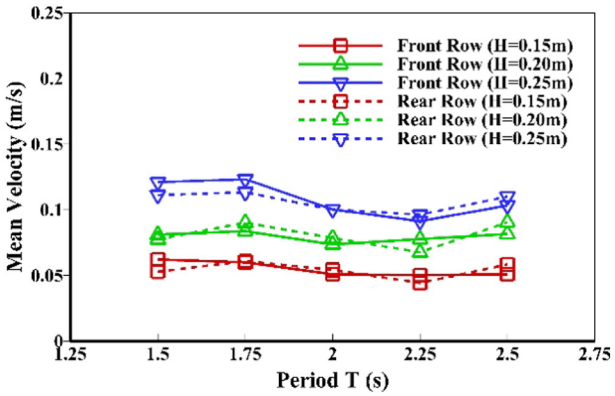

Fig. 6. Comparison of mean velocities between buoys in front and rear rows.

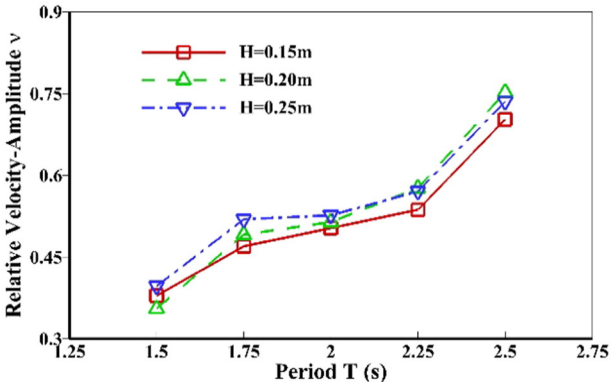

Fig. 7. Distribution of relative velocity-amplitudes.

wave conditions are below 10%. This indicates that the velocity difference between the buoys in the front and rear rows can be ignored in the numerical simulation.

Fig. 7 shows the distribution of the relative velocity-amplitudes ν, defined as the ratio of the velocity-amplitude of the heaving buoys to the velocity-amplitude of the wave elevation. The value of ν varies from 0.35 to 0.75 under the HPS effects. The distribution characteristics are correlated to the wave height. However, the amplitude increases as the incident wave period is increased. In addition, the variation of ν is more gradual between 1.75 s and 2.25 s than in other zones.

Experimental tests of HAS

A set of three accumulators was used to establish a simple HAS to experimentally verify the feasibility of the design concept. This HAS could be easily expanded to the prototype HAS with the same working pressures, which would have the desired number. The controlling strategy of the HAS as determined from in the experiments could also be used in the prototype WEC.

A schematic of HAS experiment-system is shown in Fig. 8 (a). The high-pressure oil is pumped to the accumulators by the HP station under a constant pressure and at a fixed flow rate. The upper and lower limits of the charging pressure are determined by the pre-set values of the high-low pressure switches. The charging process is stopped as soon as the higher limit is reached. During the discharging of the HAS, the oil in different accumulators is released in turn by opening the electromagnetic directional valves in the correct order. The valves are turned off once the lower limit is reached. The releasing strategy should reduce the fluctuation in the flow rate, so as to keep the rotation speed of the motor as constant as possible. The variations in the pressures in the accumulators and flow rates in the pipes are also monitored using the pressure transducers and flowmeters, respectively.

As shown in Fig. 8 (b), oil charging is operated manually using the HP station, while the discharging is done automatically using the control panel. The throttle valve and the pilot-operated pressure relief valve are used as the substitutable devices of the hydraulic motors linked to the generator. The upper and lower limits of the accumulator pressure values are set to 25.0 and 5.0 MPa, respectively. The nominal volume of the bladder accumulators is 100 L.

During the charging, the input flow rate was fixed at 15 L/min. The oil pressure was set at 12 and 13 MPa, given the capability of the HP station. The relief pressure of Valve 10 in Fig. 8 (a) varied from 5.5 to 10 MPa. The opening of the throttle valve was kept unchanged. It was observed that the charging durations under the same input pressure value were similar; the durations for the upper pressure limits of 12 and 13 MPa were approximately 10 and 10.5 min, respectively.

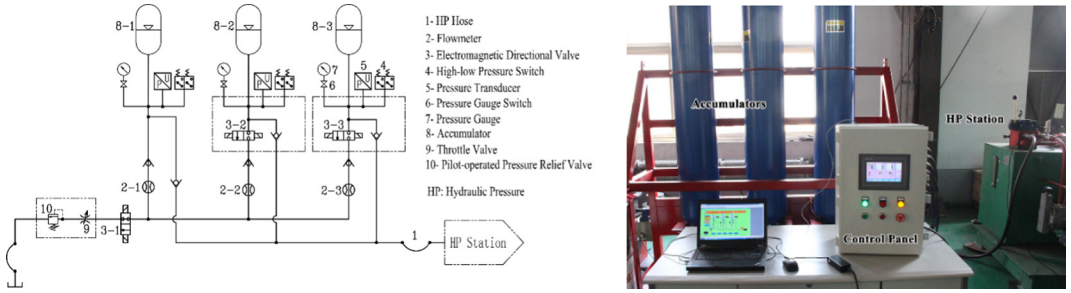

(a) System diagram (b) Testing facilities

Fig. 8. Experiment set-up of the HAS.

During the discharging process, three accumulators were triggered sequentially. First, A8-1 began to release immediately after the charging pressure reached the upper limits. Next, A8-2 and 8-3 were triggered, once the previous accumulator's flow rate decreased to a certain value (40 L/min in this study). When the discharging pressure values reached the lower limit, Valves 3-1–3-3 were then turned off sequentially. A comparison of the flow rates under the various upper/lower discharging limits is shown in Fig. 9. It can be seen that the mean flow rates increased significantly when the difference between the upper and lower limits was larger than 6 MPa. The largest flow rate was as high as 89.9 L/min. On the other hand, the maximum mean value was 54.3 L/min for the case corresponding to 13 to 5.5 MPa. It can be concluded that the primary design of the HAS was feasible and a reasonable one. Experimental tests can also provide useful data to further validate numerical models.

Numerical model

As mentioned above, the HAS divides the energy conversion process into two stages. Two parameters have to be optimized for the energy charging stage: the upper charging limit and the charging duration. The upper charging limit is actually determined by the maximum pumping forces on the ram, which is driven by the wave forces. On the other hand, the charging duration also should be considered so as to match the wave conditions. A shorter charging duration is definitely better for capturing more energy from the waves. Moreover, different control strategies for the discharging of the HAS should be tested in order to compare their effects on the final electrical power output during battery charging.

The block diagram of a wave-to-wire model that describes the conversion process of energy from wave energy to electricity is shown in Fig. 10. In the wave module, both regular and irregular waves are employed; their various parameters include the wave height, period, and spectrum. The buoy motion is simply considered to correspond to one-degree of freedom. The transfer function v(t) describes the velocities of the hydraulic rams (the oscillating velocities of the buoys under PTO effects), which can be determined based on the experimental results in Figs. 6 and 7. As a simplification, a linear-fitting equation can be employed to describe the relationship between the wave elevation velocities and the oscillating velocities of the buoys. An incident irregular wave train can be discretized to a combination of the regular waves, thereby the velocities of the rams can be derived (Ma, 2013; Qu, 2015). For the energy storage and wire modules, the governing functions and equations for the flow rate Q (t), pressure variation P(t), rotation speed n(t), torque T(t), charging voltage U(t), and current I(t) were defined based on the works of Garcia-Rosa et al. (2014) and Ghodrati and Rashid (2014).

The wave-to-wire model was implemented in the Simulink, which is run by using a script in Matlab. All the parameters could be defined and modified in the Simulink, while the dynamic simulations were carried out in Matlab. The system losses, such as those owing to friction in the pipes and devices, were also taken into account, in order to match the actual conditions.

The simulation results of the charging/discharging of a bladder accumulator (#8-1 in Fig. 8) are compared with the experimental data in Fig. 11, in order to validate the numerical model. It can be seen that the slope of the curve for the numerically determined pressure in the accumulator before 450 s is higher than that of the curve of the experimental data in Fig. 11 (a). The slope decreased subsequently, resulting in the simulated pressure reaching the upper limit (12 MPa) slightly later. In addition, the simulated pressure curve for the discharging process agreed well with experimental results. Further, as can be seen in Fig. 11 (b), the initial flow rate for the numerical model was higher than that of the real accumulator and decreased sharply till the end. Generally, the results obtained using the numerical model were in good agreements with the experimental data and can be used for further evaluating the dynamic performance of the HAS.

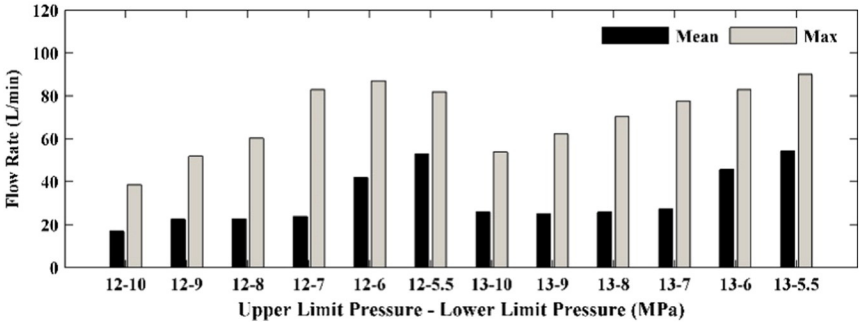

Fig. 9. Flow rates during the discharging process.

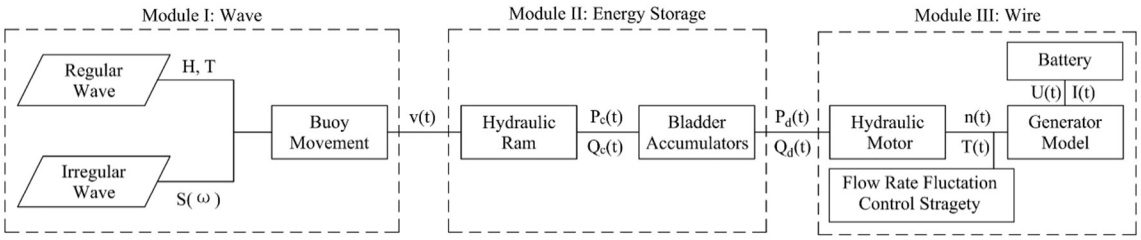

Fig. 10. Basic block diagram of the wave-to-wire model.

Simulation results

Analysis of energy-charging process

The shape of the buoys in the simulation was the same as that in the 10 kW pilot device and the model in the experiments. The shape parameters for the 100 kW final-prototype WEC are four times larger than the size of the buoys in the experiments. The significant wave height was 0.6 m and the corresponding period was 3.3 s; these were measured at the sea-trial testing site (Zhaitang Island, Qingdao). The JONSWAP has been validated as being the appropriate spectrum for the local sea area (Wu et al., 2015). The initial pressure inside the accumulator was set at 4 MPa.

The time histories of the charging parameters in one of the accumulators for regular waves (H = 0.6 m, T = 3.3 s) are shown in Fig. 12. It can be seen that the pressure in the accumulator increased rapidly for a large flow rate in the pipeline in the initial stage. With an increase in the charging time, the slopes of the curves of both the pressure and the flow rate decreased gradually. Since the numerical model in Simulink was physically ideal, the air in the bladder could be compressed infinitely under the forced pumping of the hydraulic rams. Therefore, a pressure threshold of 14.7 MPa was set as the upper limit; this was derived from the hydrodynamic analysis using the CFD software ANSYS-AQWA. The charging time was 11.6 h, at which point the pressure in the accumulator reached 14.7 MPa. This means that one buoy needed almost half a day to charge an accumulator under the existing excitation conditions.

In order to account for the effects of the actual sea conditions on the charging process, an irregular wave train was employed next. The spectrum of the wave train was validated using the data derived from the test site (see Fig. 13). The error was less than 8%. The numerical spectrum matched the real conditions well, confirming that the wave train could be used in the simulations performed next.

Two threshold values were considered for the charging process in the case of the irregular waves: 18 MPa was the nominal highest operating pressure of the hydraulic motor for the 100 kW electrical generator while 21.4 MPa was the maximum pressure that could be generated by waves of $H_{1\%}$. Therefore, 18 MPa was selected as the upper limit for the irregular waves-related calculations. Moreover, it was evident that not all the waves could drive the buoy to pump the oil. Based on the experimental data (Qu, 2015), the effective wave height was set at H = 0.15 m.

The velocities of piston-heaving, which was caused by the irregular waves are shown in Fig. 14 (a). Further, as can be seen from Fig. 14 (b), the charging time for one accumulator decreased significantly to 0.38 h (23 min). Accordingly, the time required to charge to the rated pressure (14 MPa) of the hydraulic motor was 0.22 h (13 min). The increase in the pressure curve is steeper than that in the regular waves, because the fluctuations in the irregular-waves forces were more severe. The variation in the oil flow rate was also irregular (see Fig. 14 (c)). Since the threshold of the wave excitation force kept increasing, as the time elapsed, an increasing number of waves could not pump the oil. Therefore, the generated flow rates exhibited a wide distribution in the later period.

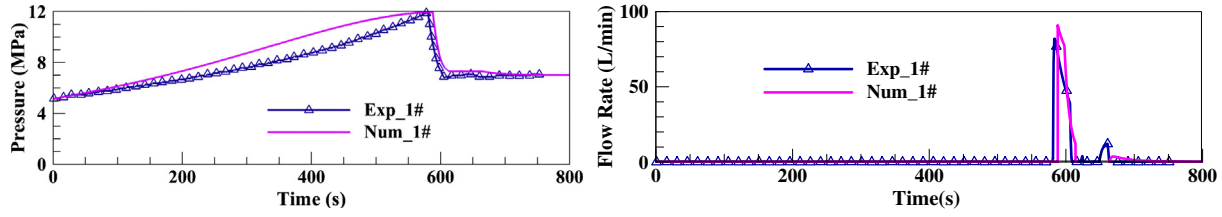

(a) Pressure variation in the accumulator (b) Discharging flow rate

Fig. 11. Comparison of energy charging and discharging process.

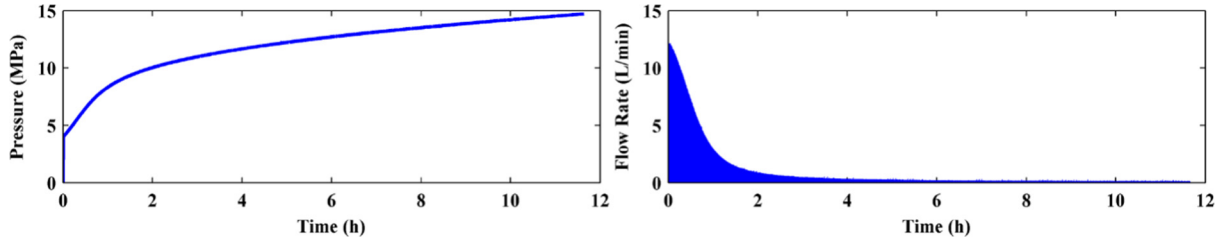

(a) Pressure variation in the accumulator (b) Flow rate variation during charging

Fig. 12. Charging process under regular wave excitation.

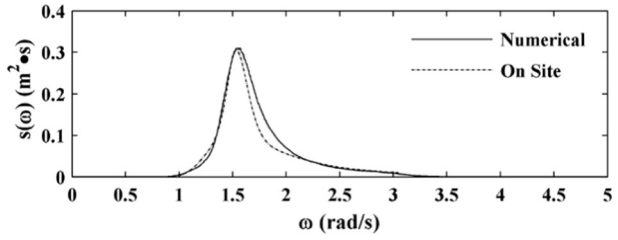

Fig. 13. Comparison and validation of wave spectrum.

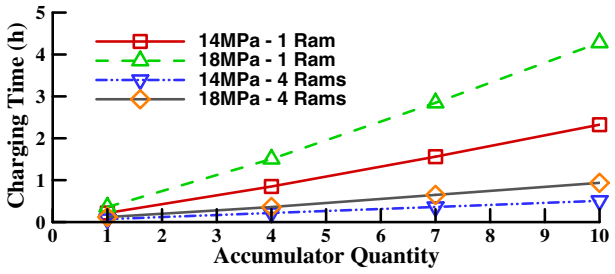

Fig. 15. Effects of the number of buoys and accumulators on the charging time.

Calculations were performed for a few more cases, in order to investigate the effects of the numbers of buoys and accumulators on the charging duration. It was assumed that each hydraulic ram was connected to just one buoy. A comparison of the obtained results is shown in Fig. 15. It can be seen that the variation in the charging time changed linearly with the number of accumulator. The buoys-array can also evidently reduce the charging time for both upper pressure limits. For ten accumulators being pumped by four buoys, the charging time reduced to 0.51 h and 0.94 h, respectively, for the two limits. Given the charging time, these numbers of accumulators and buoys were determined to be suitable for the wave conditions in effect at the test site.

Analysis of energy-discharging process

During the energy discharging of the HAS, a hydraulic motor was linked to an electrical generator (100 rpm/100 kW/690 V), which was used to charge a set of batteries (200 A·h/300 V/10% initial electric quantity). According to the generating voltage and the parameters of the batteries, the charging-voltage threshold was set to 227 V. In order to demonstrate the advantage of utilizing of the HAS, direct comparisons of the parameters related to electrical- energy-output and battery-charging between the HPS with and without the HAS are shown in Figs. 16 and 17, respectively. An irregular wave train using the spectrum in Fig. 13 was applied in the simulations. The running time of the HPS without the HAS (direct drive mode) is 627 s, which is the period of the complete energy charging and discharging process of the HPS-HAS system. The HAS included three accumulators, and the oil was released from the accumulators at the same time.

For the direct drive mode, as can be seen in Fig. 16 (a), the flow rate in the motor fluctuated severely between 0 and 200 L/min. On the contrary in Fig. 17 (a), the flow rate for the HAS was decreased gradually from 526 L/min at the start to 337 L/min at the end. The pressure in the motor was small and even the larger measurements did not exceed 0.8 MPa in Fig. 16 (b). This was caused by the rotation of the motor at the low speeds (0–28 rpm), as shown in Fig. 16 (c). The pressure for the HAS in Fig. 17 (b) was decreased from 8.1 to 2.2 MPa, and the rotation speed decreased from 71 to 48 rpm accordingly, as shown in Fig. 17 (c). In Fig. 17 (d), discrete peaks of less than 0.8 kN·m were widely distributed in the direct drive mode throughout the running-time. This caused a low battery charging-power (that peaks at 2.0 kW, see in Fig. 16 (e)). The accumulated energy in this process was only 1.9 Wh. On the other hand, the HAS generated a mild decrease in the motor-torque from 8.4 to 2.0 kN·m (see Fig. 17 (d)). Furthermore, as seen in Fig. 17 (e), the charging power was decreased mildly from 19.8 to 5.5 kW. The corresponding accumulated-energy was 76.7 Wh. Although the time for energy charging is over 20 times longer than that of discharging, the output energy of the HAS is over 40 times larger than that of the direct-drive mode. This indicates that the direct drive mode only has a disappointingly-poor effect on the performance of the energy output. It is essential to spend time on the energy charging by using the HAS.

In addition, three accumulators were used to simulate three different discharging strategies: I) discharging at the same time;

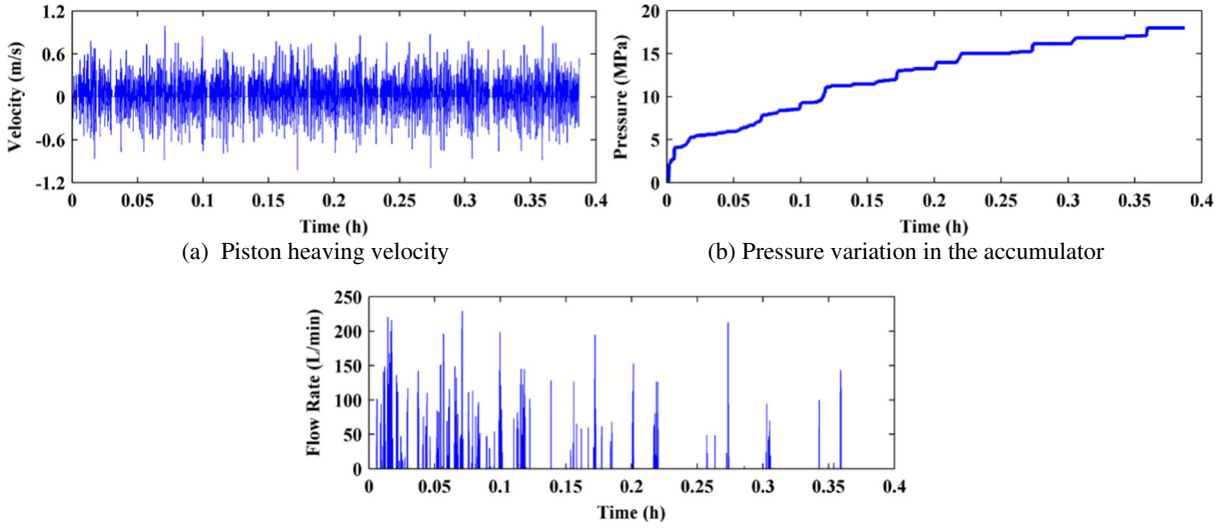

(a) Piston heaving velocity

(b) Pressure variation in the accumulator

(c) Charging flow rate

Fig. 14. Charging process under irregular wave excitation.

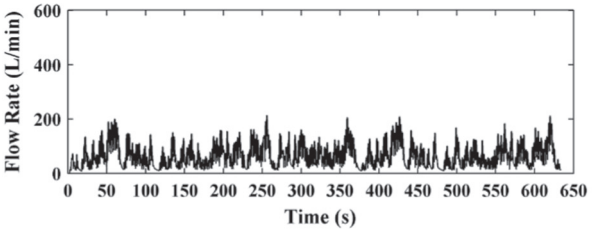

(a) Flow rate in the motor

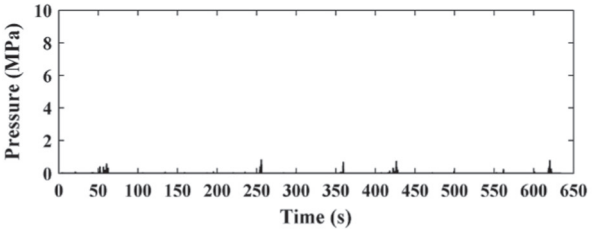

(b) Pressure in the motor

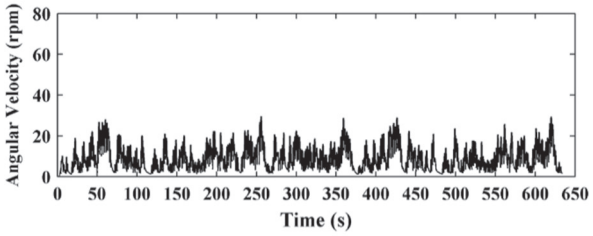

(c) Angular velocity in the motor

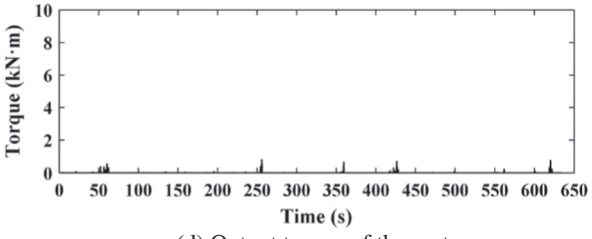

(d) Output torque of the motor

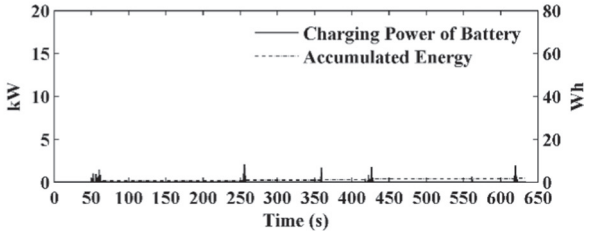

(e) Energy charged to the battery

Fig. 16. Battery charging without the HAS.

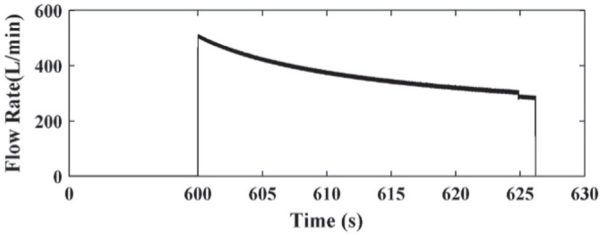

(a) Flow rate in the motor

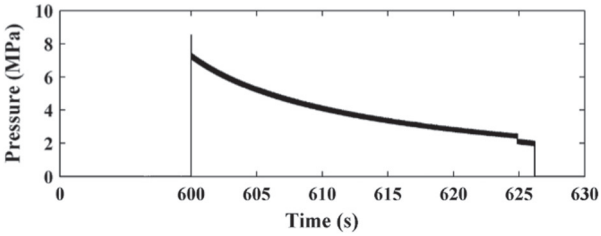

(b) Pressure in the motor

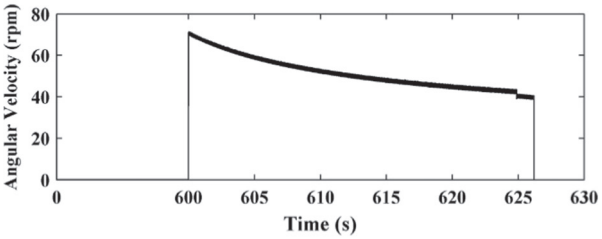

(c) Angular velocity in the motor

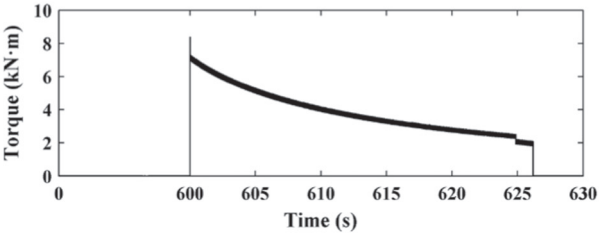

(d) Output torque of the motor

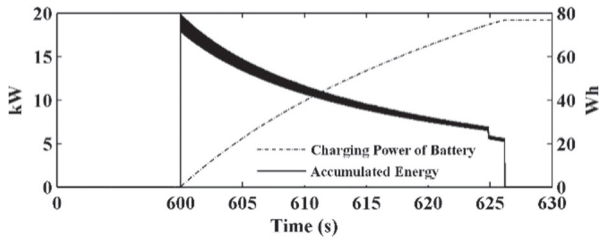

(e) Energy charged to the battery

Fig. 17. Battery charging with the HAS.

II) discharging sequentially with a flow rate trigger (240 L/min); III) discharging sequentially. The changes in the battery-charging power with time under the various strategies are shown in Fig. 18. It can be seen that the power decreased gradually under Strategy I; however, no obvious power fluctuations were observed. The discharging of only one accumulator lowered the amount of power generated because of the smaller flow rates. Compared to Strategy III, it was found that Strategy II could effectively reduce the fluctuations in the charging power. Finally, there were no evident differences in the ending times (approximately the 30th s) for the three strategies.

Additional information is listed in Table. 1. The flow rate and motor output are the mean values. Same as those in Fig. 17 (e), the battery-charging electrical energy is the integrated value. It can be seen that the motor output power was only approximately one-fifth of the installed capacity; this was owing to the low discharging flow rate. Accordingly, the amount of electrical energy delivered to the batteries in one energy storage cycle was relatively small. Thus, a greater

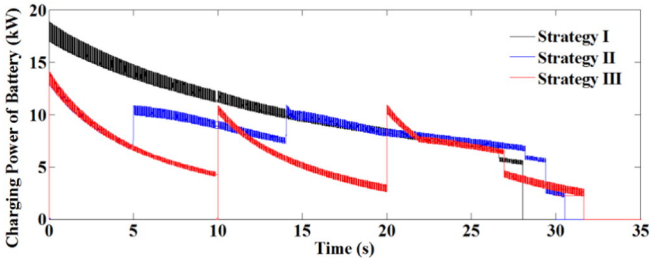

Fig. 18. Time histories of charging power under various strategies.

Table 1
Energy-discharging-related parameters.

	Strategy I	Strategy II	Strategy III
Flow rate (L/Min)	372	330	300
Motor output power (kW)	22.8	16.1	10.9
Battery electricity (Wh)	73.2	65.0	55.1

number of accumulators should be released at the same time to increase the flow rate to 536 L/min to reach the rated power output limit.

Conclusions

The wave energy density in North China is relatively small because of the sheltering effects of the island chain in the Western Pacific Ocean. The feasibility of the buoys-array type WEC for wave energy harvesting was confirmed through the sea trials of a 10 kW pilot device developed by a team at OUC.

It was found that even four buoys could not pump a constant flow rate of the oil under a high pressure to the motor. The generator was kept in the start/stop switching status under the low wave energy density at the local test site, resulting in a low operational-efficiency. The direct output voltage could not meet the battery-charging or local grid-transformation demands.

In order to fully utilize all the discrete high-pressure peaks, an energy storage system with an accumulator was designed for the 100 kW prototype WEC. The hydrodynamic experiments for the heaving buoys under the damping effects of the HAS were performed, and the relationship between the oscillating velocities of the buoys and the elevation velocities of the waves were found. The HAS was tested, and its feasibility and suitability with respect to wave energy accumulation and storage under the low-wave-energy-density conditions were evaluated.

A numerical model based on the Simulink environment of MATLAB was validated using the experimental data. It was found that the time for charging ten accumulators with four buoys was 30 min under the rated pressure of the hydraulic motor (14 MPa). In a same running time, the output energy of the HPS-HAS is over forty times larger than that of the HPS without any energy storage device. The energy discharging from three accumulators only could reach about 20 kW output power. The numbers of buoys and accumulators should be optimized to improve wave-energy storage and power generation in the future.

Acknowledgements

This work was financially supported by the “863” project (Grant No.: 2012AA052601), the National Natural Science Foundation of China (Grant No.: 41376100 and 51279185), the Shandong Natural Science Funds for Distinguished Young Scholar (Grant No.: JQ201314), the Shandong Provincial Innovation Special Project (Grant No.: 2014ZZCX06105), “111” Project (Grant No.: B14028), the Qingdao Municipal Science & Technology Program (Grant No.: 13-4-1-38-hy and 14-9-1-5-hy) and the Fundamental Research Funds for the Central Universities (Grant No.: 201564005) .

References

Abraham E, Kerrigan EC. Optimal active control and optimization of a wave energy converter. IEEE Trans. Sust Egy. 2013;4(2):324–32.
Astariz S, Iglesias G. The economics of wave energy: a review. Renew Sustain Energy Rev 2015;45:397–405.
Cargo CJ, Hillis AJ, Plummer AR. Optimisation and control of a hydraulic power take-off unit for a wave energy converter in irregular waves. Proc IMechE Part A: J Power Energy 2014;228(4):462–79.
Choi KS, Yang DS, Park SY, Cho BH. Design and performance test of hydraulic PTO for wave energy converter. Int J Precis Eng Manuf 2012;13(5):795–801.
Clement AH, Babarit A. Discrete control of resonant wave energy devices. Phil Trans R Soc A 2012;370:288–314.
Cruz J. Ocean wave energy: current status and future prespectives. 1st ed. Berlin Heidelberg: Springer; 2008.
Ekstrom R, Ekergard B, Leijon M. Electrical damping of linear generators for wave energy converters – a review. Renew Sustain Energy Rev 2015;42:116–28.
Elwood D, Yim S, Prudell J, Stillinger C, Jouanne AV, Brekken T, et al. Design, construction and ocean testing of a taut-moored dual-body wave energy converter with a linear generator power take-off. Renew Energy 2010;35:348–54.
Falcão AFO. Modelling and control of oscillating-body wave energy converters with hydraulic power take-off and gas accumulator. Ocean Eng 2007;34:2021–32.
Falcão AFO. Phase control through load control of oscillating-body wave energy converters with hydraulic PTO system. Ocean Eng 2008;35:358–66.
Falcão AFO. Wave energy utilization: a review of the technologies. Renew Sustain Energy Rev 2010;14:899–918.
Forehand DIM, Kiprakis AE, Nambiar AJ, Wallace AR. A fully coupled wave-to-wire model of an array of wave energy converters. IEEE Trans. Sust Egy. 2016;7(1):118–28.
Fusco F, Ringwood JV. A simple and effective real-time controller for wave energy converters. IEEE Trans Sust Egy 2013;4(1):21–30.
Garcia-Rosa PB, Cunha JPVS, Lizarralde F, Estefen SF, Machado IR, Watanabe EH. Wave-to-wire model and energy storage analysis of an ocean wave energy hyperbaric converter. IEEE J Oceanic Eng 2014;39(2):386–97.
Gaspar J, Calvario M, Soares CG. Pump and gas accumulator based phase control of wave energy converters. In: Soares CG, editor. Renewable energies offshore. London: Taylor & Francis Group; 2015. p. 295–303.
Ghodrati A, Rashid A. Modelling and simulation of a power take-off in connection with multiple wave energy converters. bachelor thesis. Sweden: Blekinge Institute of Technology Karlskrona; 2014.
Hansen RH, Kramer MM, Vidal E. Discrete displacement hydraulic power take-off system for the wavestar wave energy converter. Energies 2013;6:4001–44.
Haun E. Power in the waves- for multiple offshore & subsea applications. Marine technolgy reporter, Vol. 11/12; 2015. p. 1–5.
Henderson R. Design, simulation, and testing of a novel hydraulic power take-off system for the Pelamis wave energy converter. Renew Energy 2006;31:271–83.
Hodgins N, Keysan O, McDonald AS, Mueller MA. Design and testing of a linear generator for wave-energy applications. IEEE Trans Industr Electr 2012;59(5):2094–103.
Hong Y, Waters R, Bostrom C, Eriksson M, Engstrom J, Leijon M. Review on electrical control strategies for wave energy converting systems. Renew Sustain Energy Rev 2014;31:329–42.
Josset C, Babarit A, Clement AH. A wave-to-wire model of the SEAREV wave energy converter. Proc IMechE part M: J. Eng Marit Environ 2007;221:81–93.
Kelly JF, Wright WMD, Sheng WA, O'Sullivan K. Implementation and verification of a wave-to-wire model of an oscillating water column with impulse turbine. IEEE Trans Sust Egy 2015;7(2):546–53.
Lasa J, Antolin JC, Estensoro P, Santos M, Ricci P. Design, construction and testing of a hydraulic power take-off for wave energy converters. Energies 2012;5:2030–52.
Leijon M, Bernhoff H, Agren O, Isberg J, Sundberg J, Berg M, et al. Multi-physics simulation of wave energy to electric energy conversion by permanent magnet linear generator. IEEE Trans Energy Convers 2005;20(1):219–24.
Li G, Weiss G, Mueller M, Townley S, Belmont MR. Wave energy converter control by wave preidction and dynamic programming. Renew Energy 2012;48:393–402.
Lin YG, Tu L, Zhang DH, Liu HW, Li W. A study on dual-stroke pendulum wave energy conversion technology based on a water/oil integrated trasmission system. Ocean Eng 2013;67:27–34.
Liu Z, Cui Y, Zhao HY, Shi HD, Hyun BS. Effects of damping plate and taut line system on mooring stability of small wave energy converter. Math Probl Eng 2015, Article ID 814095.
Lopez I, Andreu J, Ceballos S, Alegria IM, Kortabarria I. Review of wave energy technologies and the necessary power-equipment. Renew Sustain Energy Rev 2013;27:413–34.
Ma Z. Study on hydrodynamic performance of oscillating floater buoy wave energy converter. Doctoral Thesis: Ocean University of China; 2013 [In Chinese].
Melo AB, Huckerby J. 2011 annual report. The executive committee of ocean energy systens; 2011.
National Ocean Technology Center (NOTC). Technology progress of Chinese marine energy. 1st ed. Beijing: Ocean Press; 2014 [In Chinesse].
Nie ZX, Xiao X, McMahon R, Clifton P, Wu Y, Shao SY. Emulation and control methods for direct drive linear wave energy converters. IEEE Trans Indust Info 2013;9(2):790–8.
Pizer DZ, Retzler C, Henderson RM, Cowieson FL, Shaw MG, Dickens B, et al. Pelamis WEC—recent advances in the numerical and experimental modelling programme. Proceedings of 6th European wave tidal energy conference Glasgow, UK; 2005. p. 373–8.
Polinder H, Damen MEC, Gardner F. Design, modeling and test results of the aws pm linear generator. Eur Tran Electr Power 2005;15:245–56.
Qu N. Study on hydrodynamic performance of oscillating buoy WEC considering power take-off system. Master Thesis: Ocean University of China; 2015 [In Chinese].
Sheng W, Alcorn R, Lewis A. On improving wave energy conversion, part I: Optimal and control technologies. Renew Energy 2014;75:922–34.
Sheng W, Alcorn R, Lewis A. On improving wave energy conversion, part II: Development of latching control technilogies. Renew Energy 2015;75:935–44.

Shi HD, Cao FF, Liu Z, Qu N. Theoretical study on the power take-off estimation of heaving buoy wave energy converter. Renew Energy 2016;86:441–8.
Stratigaki V, Troch P, Stallard T, Forehand D, Kofoed JP, Folley M, et al. Wave basin experiments with large wave energy converter arrays to study interactions between the converters and effects on other users in the sea and the coastal area. Energies 2014;7:701–34.
Titah-Benbouzid H, Benbouzid M. Ocean wave energy extraction: up-to-date technologies review and evaluation. International power electronics and application conference and exposition, shanghai, China; 2014. p. 338–42.
Wu SP, Liu CY, Chen XP. Offshore wave energy resource assessment in the East China Sea. Renew Energy 2015;76:628–36.
Zhang DH, Li W, Lin YG, Bao JW. An overview of hydraulic systems in wave energy application in China. Renew Sustain Energy Rev 2012;16:4522–6.
Zhang YQ, Sheng SW, You YG, Wu BJ, Liu Y. Research on energy conversion system of floating wave energy converter. China Ocean Eng 2014;28(1):105–13.